Identification of Tertiary Base Pair Resonances in the Nuclear Magnetic Resonance Spectra of Transfer Ribonucleic Acid†

Brian R. Reid,* Lillian McCollum, N. Susan Ribeiro, Joseph Abbate, and Ralph E. Hurd

ABSTRACT: The low-field hydrogen-bond ring NH proton nuclear magnetic resonance (NMR) spectra of several transfer ribonucleic acids (tRNAs) related to yeast $tRNA^{Phe}$ have been examined in detail. Several resonances are sensitive to magnesium ion and temperature, suggesting that they are derived from tertiary base pairs. These same resonances cannot be attributed to cloverleaf base pairs as shown by experimental assignment and ring current shift calculation of the secondary base pair resonances. The crystal structure of yeast $tRNA^{Phe}$ reveals at least six tertiary base pairs involving ring NH hydrogen bonds, which we conclude are responsible for the extra resonances observed in the low-field NMR spectrum. In several tRNAs with the same tertiary folding potential and dihydrouridine helix sequence as yeast $tRNA^{Phe}$, the extra resonances from tertiary base pairs are observed at the same position in the spectrum.

The recent determination of the crystal structure of yeast $tRNA^{Phe}$ (Kim et al., 1974a,b; Robertus et al., 1974; Sussman & Kim, 1976; Stout et al., 1978) has stimulated a variety of physical and biochemical studies on the conformation and dynamics of tRNA in solution. One of the most useful approaches to this problem has been high-resolution nuclear magnetic resonance (NMR)[1] studies on the hydrogen-bonded ring NH protons of complementary base pairs. Only the ring NH proton is sufficiently deshielded to move into the extreme low-field region (−11 to −15 ppm) of the NMR spectrum (Katz & Penman, 1966). In tRNA these hydrogen-bonded protons have quite long helix lifetimes (Englander & Englander, 1965), and this permits them to be detected in the low-field NMR spectrum in H_2O solvents despite the enormous water resonance at ca. −4.6 ppm (Kearns et al., 1971a,b; Shulman et al., 1973; Kearns & Shulman, 1974). Since each base pair contains only one ring NH hydrogen bond, the number of resonances in the extreme low-field spectrum should correspond to the number of stable base pairs in solution. Until recently the low-field NMR spectra of several tRNA species have been interpreted to contain only 19 to 20 resonances derived exclusively from secondary base pairs in the cloverleaf structure (Jones & Kearns, 1974, 1975; Wong et al., 1975a–c; Jones et al., 1976). Theoretical arguments justifying the absence of detectable additional resonances have been presented by Kearns & Shulman (1974).

Over a year ago we were able to show, using highly resolved spectra of extremely pure tRNA, that the NMR spectrum of *Escherichia coli* $tRNA_1^{Val}$ contains 27 resonances between −11 and −15 ppm (Reid & Robillard, 1975); 20 of these are derived from secondary structure with an additional 6 to 7 resonances from tertiary base pairs and GU pairs. A similar conclusion concerning the low-field spectrum of $tRNA^{fMet}$ was reported by Daniel & Cohn (1975). We have extended our study to encompass 14 different class 1 tRNAs containing 20 ± 1 standard secondary base pairs; in all cases we observed 7 ± 1 additional base pairs from three-dimensional folding (Reid et al., 1977). Despite this overwhelming evidence there remains some disagreement concerning the extent to which tertiary base pair resonances can be detected in tRNA low-field spectra (Bolton & Kearns, 1976; Reid, 1976; Bolton et al., 1976; Kearns, 1976).

It is obvious that accurate assignment of the tertiary base pair and secondary base pair resonances in the NMR spectrum would establish an extremely valuable tool with which to monitor structural perturbations and conformational dynamics of tRNA in solution. The first step in such a procedure is to establish which resonances in a given spectrum are derived from tertiary base pairs and which are derived from the cloverleaf structure. The purpose of this paper is to establish, by several independent methods, which resonances in the spectra of several different tRNAs are derived from tertiary interactions. In subsequent papers (Hurd & Reid, 1979a,b; Hurd et al., 1979) we will assign the extra NMR resonances to specific three-dimensional interactions.

Materials and Methods

Purification of tRNA. *E. coli* $tRNA_1^{Val}$, $tRNA_m^{Met}$, $tRNA_1^{Arg}$, and $tRNA^{Phe}$ as well as yeast $tRNA^{Phe}$ were purified by a combination of BD-cellulose chromatography (Gillam et al., 1967), DEAE-Sephadex A50 chromatography (Nishimura, 1971), and Sepharose 4B chromatography (Holmes et al., 1975) as described previously (Reid et al., 1977). The purity of each tRNA was established from the molar stoichiometry of aminoacylation by using an excess of the appropriate aminoacyl-tRNA synthetase; all of the tRNAs used in this study were chargeable to greater than 1760 pmol of amino acid/A_{260} unit. The isoacceptor identity was established by two-dimensional fingerprinting of complete RNase T_1 digests of the tRNA. Prior to NMR spectroscopy, each tRNA was dialyzed twice against 12 L of 0.1 mM sodium thiosulfate, pH 7.0, and then lyophilized in 120 A_{260} (6 mg) aliquots.

NMR Spectra. Six milligram aliquots of tRNA were dissolved in 0.19–0.20 mL of the appropriate buffer to give final concentrations of ~1.2 mM tRNA. The sample was then transferred to an NMR microtube (Wilmad Glass Co.)

† From the Biochemistry Department, University of California, Riverside, California 92521. *Received August 10, 1978; revised manuscript received May 29, 1979.* This work was supported by grants from the National Cancer Institute, Department of Health, Education and Welfare (CA11697), the National Science Foundation (PCM73-01675), and the American Cancer Society (NP-191). The high-resolution spectra were obtained on a Bruker HXS-360 spectrometer at the Stanford Magnetic Research Laboratory supported by National Science Foundation Grant No. GR23633 and National Institutes of Health Grant No. RR00711.

[1] Abbreviations used: DHU, dihydrouridine; rT, ribothymidine; m^7G, N^7-methylguanosine; Ψ, pseudouridine; EDTA, ethylenediaminetetraacetic acid; NMR, nuclear magnetic resonance; tRNA, transfer ribonucleic acid; BD-cellulose, benzoylated DEAE-cellulose.

0006-2960/79/0418-3996$01.00/0

containing a 5-mm diameter × 9-mm height sample compartment. Spectra were taken on a Bruker HXS-360 spectrometer at the Stanford Magnetic Resonance Laboratory and were accumulated by using correlation spectroscopy (Dadok & Sprecher, 1974). The sweep parameters were 2500 Hz in 0.8 s with a 0.2-s delay between sweeps. After 1000 sweeps the spectra were correlated and printed out directly onto 8.5 × 11 in. paper with the x axis usually being scaled to 90 Hz/cm. Chemical shifts are expressed in parts per million from the reference DSS (2,2-dimethylsilapentane-5-sulfonate); they were experimentally determined with respect to the H_2O peak, to which was added the known chemical shift of water from DSS at that temperature.

Isolation of Hairpin Fragments. Cleavage of tRNA at G20, or at G20 and G57, was carried out by controlled partial RNase T_1 digestion and separation of the resulting fragments on Sephadex G100, as described previously (Reid et al., 1972). The identity of each fragment was confirmed by fingerprinting. Fragment 1–45 and fragment 47–76 were produced by cleaving the tRNA at m^7G46 by using the procedure of Simsek et al. (1973). The reaction mixture was placed on a Sephadex G100 column at 65 °C, and the two fragments were separated as described previously (Reid et al., 1972). As expected, the larger fragment contained s^4U and the smaller, later eluting, fragment did not; the fragments were further characterized by RNase T1 fingerprinting. The fragments were dialyzed against distilled water and lyophilized.

Results

We have used several approaches to establish which resonances in tRNA low-field spectra are not derived from the secondary cloverleaf structure. The first method involved identifying which resonances are most sensitive to temperature, and these can be eliminated from the spectrum at elevated temperature in tRNA species with stable cloverleaf helixes. A second approach involves analysis of resonances which shift as a function of magnesium ion at constant temperature. A completely independent approach we have used is to calculate the predicted resonance position of all secondary base pairs in the cloverleaf structure by using a combination of the known nearest neighbors and next-to-nearest neighbors together with ring current shifts from these proximal bases and the crystallographically determined screw pitch of the tRNA secondary helixes. This approach indicates subtractively which of the experimentally observed resonances are additional interactions derived from tertiary base pairs. Finally, in several cases we have experimentally assigned the secondary base pair resonances from the NMR spectra of helical hairpin fragments dissected out of that tRNA species.

The results of temperature-dependent studies of *E. coli* $tRNA_1^{Val}$ are shown in Figure 1. At 45 °C (upper spectrum) there are 20 peaks between −11 and −15 ppm containing a total of 27 protons from 27 base pairs (peaks C and O contain 2 protons, the H–I–J complex contains 5 protons, and L contains somewhat more than 4 protons). Upon raising the temperature of 55 °C, one observes a discrete intensity loss by broadening from peaks A (−14.9 ppm), B (−14.3 ppm), G (−13.4 ppm), I (−12.9 ppm), O (−12.2 ppm), and S (−11.5 ppm). In addition, there is a slight intensity loss from peak C, peak E coalesces into F, and peak P coalesces into O. These losses, including the three protons between −10.6 and −9.4 ppm, reflect the early destabilization of the weakest interactions in the solution structure.

The effect of magnesium on the solution structure is shown in Figure 2. The top spectrum is that of *E. coli* $tRNA_1^{Val}$ in the complete absence of magnesium ion in a buffer con-

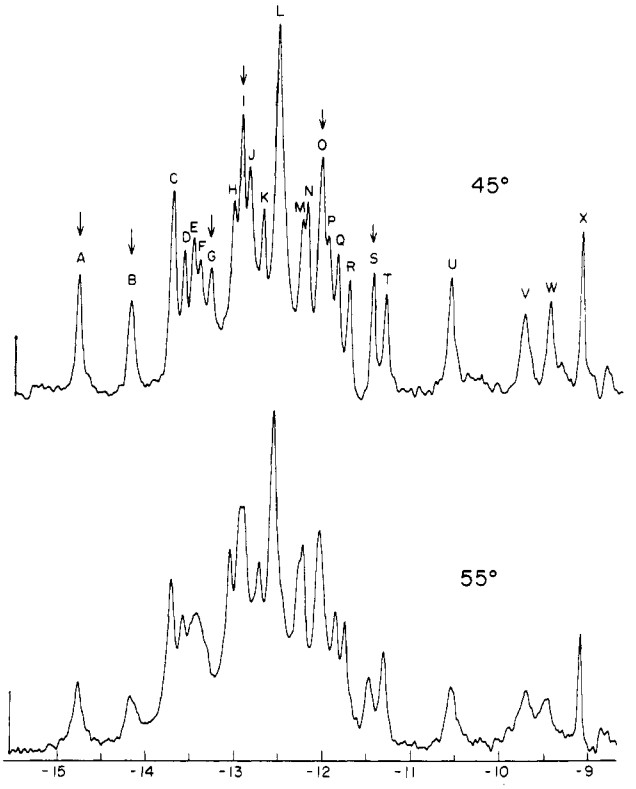

FIGURE 1: The 360-MHz low-field proton NMR spectra of pure *E. coli* $tRNA_1^{Val}$ in 10 mM sodium cacodylate, 10 mM EDTA, and 9 mM $MgCl_2$, pH 7.0. As the temperature is raised, intensity loss and broadening are observed in peaks A, B, G, I, O, and S (as well as peaks U, V, and W) while peaks J and P move downfield. At 35 °C peaks A and B have equal intensity.

taining 10 mM EDTA (8–10-fold molar excess over tRNA). As one adds magnesium chloride to 2 mM (EDTA/Mg/tRNA = 10:2:1) one observes that peak E and peak J move downfield slightly. Further addition of magnesium chloride to 9 mM (EDTA/Mg/tRNA = 10:9:1) produces further shifting of peaks E and J as well as small shifts in peaks O, P, and Q. This rearrangement at around −12.1 ppm appears to be an upfield shift of one of the protons in peak O and a downfield shift of P, although it is difficult to state precisely which peaks move and which remain stationary. In the presence of small amounts of residual magnesium (no EDTA), peak E continues its downfield journey; one proton in peak L moves slightly upfield, peak Q moves downfield, and one of the two protons in peak O moves slightly downfield (see Figure 2d). Finally, in the presence of excess magnesium ion (15 mM) peak E has moved all the way over to peak D, peak J (and peak H) has coalesced with I, and the O–P–Q complex has rearranged into four single protons. We are not yet in a position to precisely interpret these structural changes; however, it is nevertheless apparent that magnesium-sensitive resonances occur in the spectrum at −13.5, −12.9, and ca. −12.2 ppm. The other three peaks which showed temperature sensitivity in Figure 1 (peaks A, B, and S) remain relatively unmoved by magnesium deprivation. Although the spectral regions in which these shifts occur are relatively crowded, it appears that the transitions involve the smooth shifting of a whole integral proton from one extreme position to the other extreme position, i.e., a process in the fast-exchange limit of the NMR time scale. Although not conclusive, a possible explanation of this observation is that magnesium ion is changing the population distribution of two conformational states of tRNA which interconvert moderately rapidly ($\sim$1000 s^{-1}).

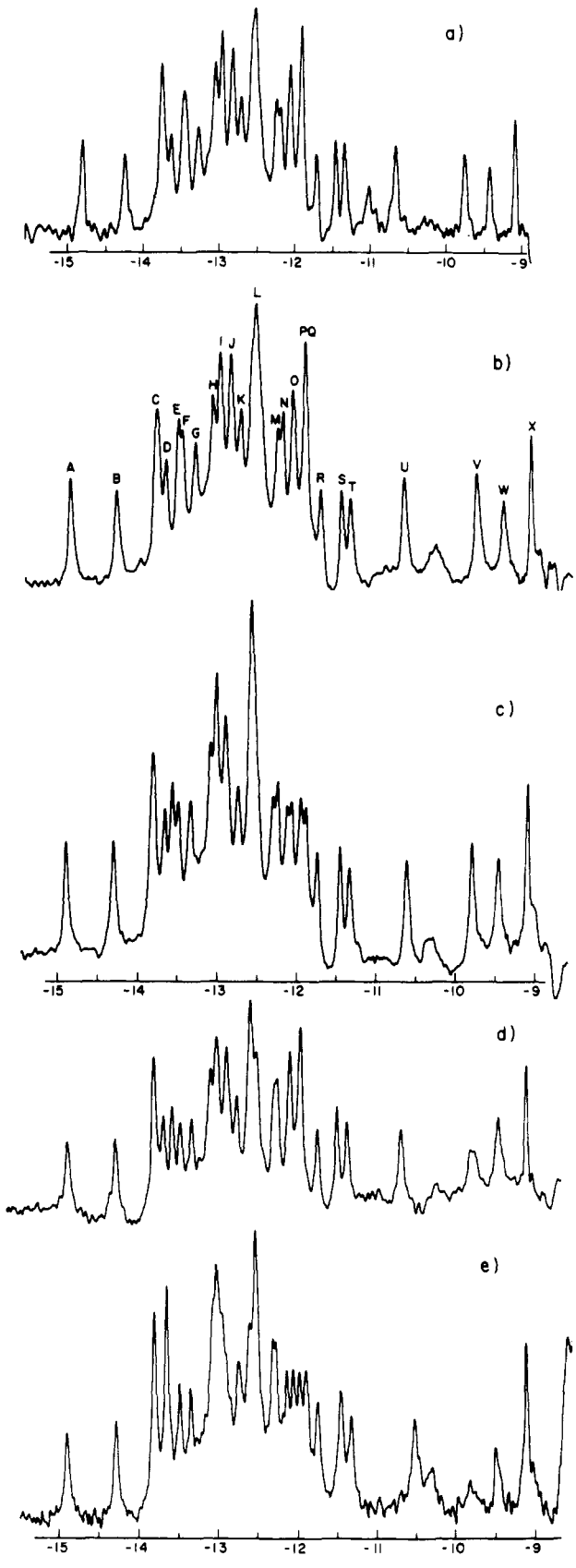

FIGURE 2: NMR spectra of *E. coli* $tRNA_1^{Val}$ at various magnesium ion and buffer concentrations. All spectra are at 35–38 °C: (a) 10 mM sodium cacodylate and 10 mM EDTA, pH 7.0; (b) same as in part a plus 1.6 mM $MgCl_2$; (c) same as in part a plus 9 mM $MgCl_2$; (d) 5 mM sodium phosphate and 100 mM NaCl, pH 7.0; the sample was prepared by dialysis against water and may contain traces of residual bound magnesium; (e) 10 mM sodium cacodylate, 100 mM NaCl, and 15 mM $MgCl_2$, pH 7.0.

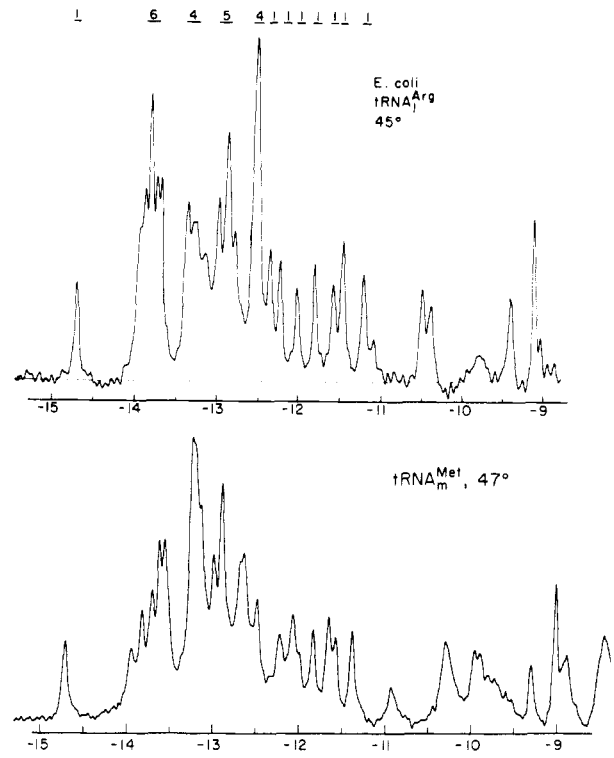

FIGURE 3: Low-field NMR spectra of *E. coli* $tRNA_1^{Arg}$ and *E. coli* $tRNA_m^{Met}$ in 10 mM sodium cacodylate, 100 mM NaCl, and 15 mM $MgCl_2$, pH 7.0. The strong ring current of purines requires that a minimally shifted AU resonance be in an environment with pyrimidines occupying the 3′ above and 5′ below positions. Examples are UA30 and AU50 in $tRNA_m^{Met}$ and UA4 in $tRNA_1^{Arg}$ (see Figure 13). Note that, apart from the s^4U8 resonance at ca. −14.8 ppm (see next paper), neither of the spectra contain a resonance below −14.0 ppm.

Having established the presence of magnesium-sensitive and temperature-sensitive resonances in the spectrum, we next attempted to determine which resonances were derived from secondary cloverleaf base pairs. Our first approach was to use the known base pairing sequence of a tRNA combined with the upfield ring current shift parameters from neighboring nucleotides. The net upfield ring current shift on a given ring NH proton depends upon both the angle and the distance of the neighboring bases and hence is extremely sensitive to three-dimensional structure. Ring current shift parameters for base pairs in tRNA have been reported by Shulman et al. (1973) from empirical analyses of observed lines in tRNA spectra. These values have been revised somewhat by Kearns and Wong (Kearns, 1976; Kearns & Wong, 1975). We have found these ring current shift parameters to be singularly inadequate in predicting tRNA spectra. In the case of many tRNAs, resonances are predicted at positions up to 0.5 ppm removed from the nearest experimentally observed resonance. Two examples are shown in Figure 3. In the case of *E. coli* $tRNA_m^{Met}$, the Kearns shift rules (Kearns, 1976) predict AU50 at −14.2 ppm and UA30 at −14.2 ppm; experimentally, the nearest resonances are observed at −14.75 and −13.9 ppm. Similarly, in *E. coli* $tRNA_1^{Arg}$ these rules predict UA4 at −14.2 ppm, although the nearest experimental resonances are at −14.75 or −13.9 ppm. A major fault in the derivation of these empirical shift values was the assumption that all observed lines in tRNA spectra are derived only from the 20 secondary cloverleaf base pairs. Further errors derived from neglecting second-order next-to-nearest neighbor effects and the assumption that tRNA helixes have 12-fold A′ RNA geometry when in fact they have a screw pitch similar to 11-fold A RNA geometry (Sussman & Kim, 1976). We have had much more

Table I: Combined Nearest and Next-to-Nearest Neighbor Shifts on Secondary Base Pairs in *E. coli* $tRNA_1^{Val}$

base pair	net shift[a] (ppm)	resonance position[b] (ppm)	order of resonances in secondary spectrum (ppm)
GC1	+1.17?	−12.28?	UA12, −13.8
GC2	+0.71	−12.74	UA29, −13.8
GC3	+0.41	−13.04	AU6, −13.7
UA4	+0.63	−13.72	UA4, −13.7
GC5	+1.68	−11.77	UA7, −13.6
AU6	+0.62	−13.73	
UA7	+0.75	−13.60	GC53, −13.1
			CG11, −13.1
GC10	+0.9?	−12.6?	GC3, −13.0
CG11	+0.38	−13.07	CG51, −12.9
UA12	+0.55	−13.80	CG28, −12.8
CG13	+1.45?	−12.0?	GC31, −12.8
			GC2, −12.7
CG27	+0.91?	−12.54?	GC52, −12.6
CG28	+0.61	−12.84	GC10, −12.6?
UA29	+0.57	−13.78	CG27, −12.5?
CG30	+1.10	−12.35	CG30, −12.4
CG31	+0.61	−12.84	GC1, −12.3?
			GC49, −12.2
CG49	+1.23	−12.22	
GU50	?	?	CG13, −12.0?
CG51	+0.57	−12.88	
GC52	+0.88	−12.57	CG5, −11.7
GC53	+0.31	−13.14	

[a] The summed shifts from neighboring nucleotides on the ring NH proton were calculated by using the 11-fold helix parameters of Arter & Schmidt (1976). [b] Offset values of AU° = −14.35 ppm and GC° = −13.45 ppm (required to account for fragment spectra) were used to determine the shifted resonance position.

success in predicting our tRNA spectra and helical hairpin fragment spectra by using the nearest neighbor and next-to-nearest neighbor ring current shifts for 11-fold RNA helixes reported by Arter & Schmidt (1976). In Table I we show a detailed tabulation of these ring current shifts for the cloverleaf structure of *E. coli* $tRNA_1^{Val}$, the sequence of which is shown in Figure 13. The second column lists the combined first-order and second-order ring current shifts on each base pair from its stacked neighbors. In the case of terminal base pairs (especially external termini) there is obviously uncertainty concerning the position of the next stacked nucleotide. In these cases we have estimated these ring current effects based on the crystal structure stacking diagram of yeast $tRNA^{Phe}$ (Sussman & Kim, 1976) and designated such base pair resonances with a question mark. We have further assumed that base pairs 7 and 49 mutually shift each other and that residues 26 and 44 are stacked between base pairs 10 and 27 as seen in the crystal structure. In the third column the AU base pairs are listed first in order of increasing upfield neighboring shifts. The main reason for listing AU pairs at the low-field end of the spectrum is that U N3H is inherently more deshielded than G N1H, as is shown in Figure 4. In addition, the G N1H in a GC pair only suffers a minor downfield shift from the weak ring current of C, whereas the U N3H suffers a large downfield shift from the strong in-plane ring current of A, thus further ensuring that AU pairs resonate at lower field than GC pairs. The next parameter which must be determined is the starting position of an isolated unshifted AU resonance (AU°). This was solved experimentally from the observed spectra of several tRNAs and helical fragments. As shown in Table I, the five AU pairs experiencing the smallest upfield shift are base pairs 12, 29, 4, 6, and 7; their upfield shifts are between 0.55 and 0.75 ppm, and these five resonances should be observed within 0.2 ppm of each other. In the experimental spectrum in Figure 5, the lowest field

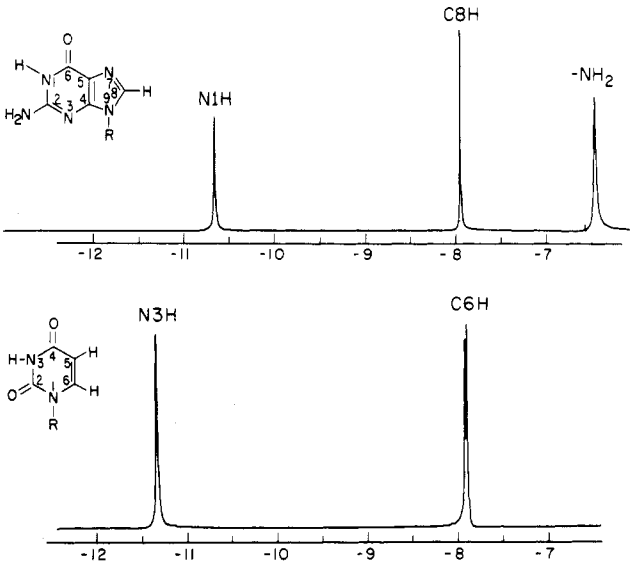

FIGURE 4: Low-field portion of the NMR spectra of guanosine and uridine in dry Me_2SO. The uridine N3H resonates 0.7 ppm lower field than the guanosine N1H. Upon forming complementary base pairs, the G N1H suffers a weak downfield shift from the in-plane cytosine whereas the U N3H suffers a stronger downfield shift from the in-plane adenine, thus further separating these resonances.

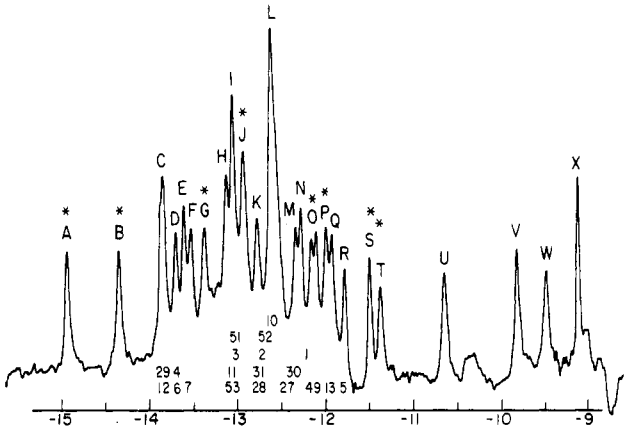

FIGURE 5: Assigned NMR spectrum of *E. coli* $tRNA_1^{Val}$. The secondary Watson–Crick resonances are designated by their cloverleaf base pair numbers; extra resonances are designated by asterisks. The secondary assignments were made on the basis of defined hairpin fragment spectra and ring current shift calculations calibrated on these model helixes. Possibly serious ambiguities exist for terminal base pairs 13 (concerning A14) and 1 (concerning A73); uncertainties in predicting CG31 (concerning C32) and GC53 (concerning T54) are less serious due to the weak ring current of pyrimidines.

grouping of five such resonances is the two-proton peak at −13.8 ppm and the three single protons between −13.7 and −13.5 ppm (analysis of hairpin fragment spectra shown later confirms that UA29 and UA12 do in fact resonate between −13.7 and −13.9 ppm). Hence, these AU resonances must have started at −14.35 ppm. Analysis of several other tRNAs and small AU-containing helixes confirms this value of −14.35 ppm for AU°. Similar treatment of the experimental spectra of GC-containing hairpin helixes leads to a value close to −13.4 ppm for GC°. In some cases a value for GC° of −13.45 ppm appears superior, whereas in other cases a value around −13.35 ppm gives a better fit to the data. In view of the uncertainty in the upfield ring current shift, we are not in a position to state the precise value of GC°; any of the above values predict our observed resonances with an accuracy of ±0.1 ppm. The results of this treatment on the 20 Watson–Crick cloverleaf base pairs of *E. coli* $tRNA_1^{Val}$ lead to the secondary as-

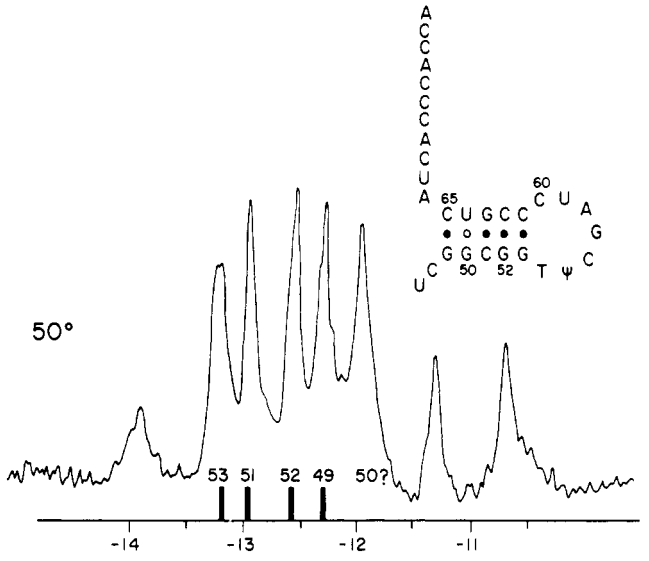

FIGURE 6: Spectrum of the isolated rT helix of *E. coli* $tRNA_1^{Val}$ at 50 °C in 5 mM sodium phosphate and 100 mM NaCl, pH 7.0. Assignment of the four GC pairs is based on ring current shift effects discussed in the text.

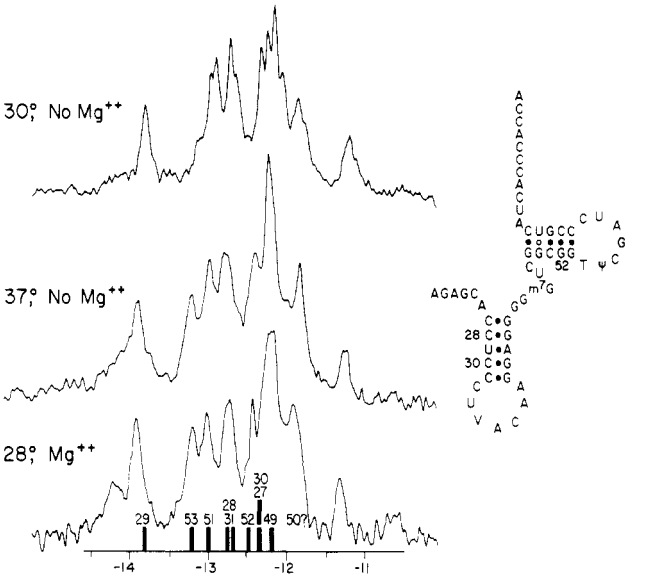

FIGURE 7: Spectra of fragment 20–76 containing the anticodon helix and the rT helix of *E. coli* $tRNA_1^{Val}$ at various temperatures in the presence and absence of magnesium. The assignments are discussed in the text.

signments shown in Figure 5. It is obvious that peaks A and B are not assignable to the cloverleaf structure. There are six protons observed between −13.8 and −13.4 ppm, whereas only five cloverleaf resonances are predicted. Thus, there is one resonance from tertiary base pairing in this region and we assign the extra resonance to peak G on the basis of the temperature lability of this resonance. The H–I–J complex at ca. −13 ppm contains five protons by integration and by computer simulation. There are only four cloverleaf resonances predicted at this position, and hence the complex H–I–J peak probably also contains a tertiary resonance. Peak L contains slightly over four protons, and at least four cloverleaf resonances are predicted near this position—although uncertain, it could conceivably contain a tertiary resonance. Between −12.4 and −11.7 ppm there are obviously seven protons in the spectrum; only five secondary base pairs are predicted in this region if CG27 is assumed to be in peak L. Our predictive accuracy is inadequate to state which peaks are the extra two resonances; however, they are unlikely to be peaks M or N. The assignment of secondary base pair CG13 is uncertain; it resonates somewhere between −12.4 and −11.6 ppm (depending on the upfield shift by A14). Independent evidence in a following paper (Hurd et al., 1979) indicates that CG13 in the A14, UA12 environment resonates at −12.05 ppm. GC5 suffers a large neighboring ring current shift (1.68 ppm), and this is reasonably accounted for by peak R; however, an error of only 15% in calculating the shift on GC5 could change this assignment. Regardless of this slight ambiguity, there are obviously extra resonances not derived from secondary Watson–Crick pairs at −11.5 and −11.4 ppm. The experimental spectrum thus appears to contain extra resonances at −14.9, −14.3, −13.4, −12.85, −12.2, −12.0, −11.5, and −11.4 ppm. These positions are encouragingly close to many of the observed temperature-sensitive and magnesium-sensitive resonances described earlier.

Despite the agreement between experiment and theory in the foregoing prediction of cloverleaf resonances, we realized that the uncertainties in this approach would benefit from experimental refinement. Consequently, we decided to investigate the NMR spectra of several hairpin helical fragments derived from tRNA, especially $tRNA_1^{Val}$. Our goals were twofold: first, to produce several simple unequivocal spectra upon which to test the predictive ring current shift values of Arter & Schmidt (1976) and, secondly, to *experimentally* assign the individual base pairs in each of the cloverleaf helixes. Figure 6 shows the spectrum of the 47–76 fragment residue of $tRNA_1^{Val}$ containing the isolated rT helix. At the bottom of the spectrum are shown the positions of base pairs 49, 51, 52, and 53 predicted according to the Arter & Schmidt values for 11-fold helixes. It is apparent that the predictions for the four Watson–Crick base pairs account for four of the experimental lines quite well. It should be remembered that in the fragment the terminal base pairs 49 and 53 may not experience the full ring current shift which they experience in the intact tRNA. There is a small broadened resonance at −13.95 ppm which disappears completely upon raising the temperature by 5 °C; it is probably derived from a weak base pair (a bulge pair) between A66 and U47. More interesting is the unpredicted peak at −11.95 ppm from G50–U64 (probably U64 N3H); the two half-proton peaks at −11.35 and −10.7 ppm are presumably from G50 N1H, although we are at a loss to explain why this proton is split into two distinct environments. However, these three peaks at the high-field end (two protons) are related to GU50 and will be discussed in more detail in a separate manuscript on GU wobble base pairing. Thus, this hairpin helix spectrum corroborates the resonance positions predicted theoretically according to the procedure outlined earlier and *experimentally* assigns base pairs 53, 51, 52, and 49 to the positions shown. An additional point of interest is that the resonance from the tertiary base pair T54–A58 can be observed in this isolated fragment upon cooling to low temperature as shown in the following paper (Hurd & Reid, 1979a).

The spectra of $tRNA_1^{Val}$ fragment 21–76 containing the anticodon helix in addition to the rT helix are shown in Figure 7. Resonances already assigned to base pairs 53, 51, 52, and 49 (plus the GU-associated intensity at −11.95 and −11.35 ppm) are observed as before at their expected positions; additional intensity is also observed at −13.9, −12.8, −12.7, and −12.35 ppm. At the bottom of Figure 7 it can be seen that the additional intensity can be accounted for by the predicted five base pairs of the anticodon helix, namely, base pairs 29, 31, 28, 27, and 30, respectively. To corroborate the subtractive

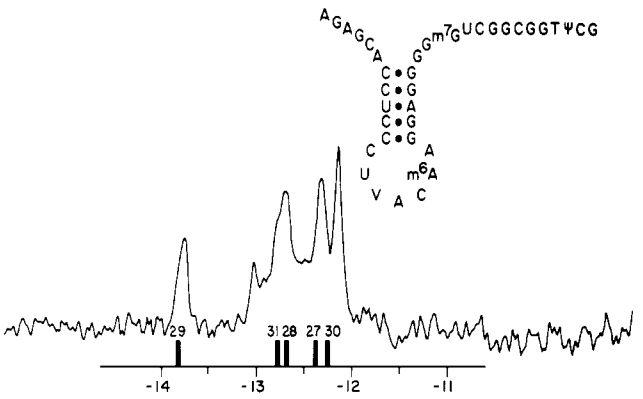

FIGURE 8: NMR spectrum of fragment 20–57 of *E. coli* $tRNA_1^{Val}$ containing the anticodon helix. The bars of the *x* axis are the resonance positions predicted from ring current shift effects as described in the text.

assignment of the anticodon helix, we prepared fragment 21–57 containing the isolated anticodon stem. As shown in Figure 8, the spectrum of the anticodon helix alone nicely accounts for the additional intensity in Figure 7 compared to Figure 6. Thus, both subtractively and directly we can assign base pairs 29, 31, 28, 27, and 30 as indicated. In all cases the agreement between observed resonances and resonances predicted on 11-fold helical geometry using published ring current values (Arter & Schmidt, 1976) together with AU° = −14.35 ppm and GC° = −13.45 ppm is remarkably good.

We have not analyzed the spectrum of the DHU stem alone, but Figure 9 shows the spectra of this helix together with the five base pairs of the anticodon helix in fragment 1–45 of $tRNA_1^{Val}$. At 37 °C the spectrum contains the expected anticodon helix plus additional intensity at −13.95, −13.3, −12.55, and −11.8 ppm. We attribute this additional intensity to base pairs 12, 11, 10, and 13, respectively. The agreement between the observed position of DHU stem resonances in isolated fragments, their predicted positions based on 11-fold helix geometry, and their deduced positions in intact tRNA is not as good as in other helixes. In several DHU stem fragment spectra we observe base pairs 12, 11, and 10 somewhat downfield of their expected positions. We attribute these differences to the fact that the DHU stem geometry is distorted in intact tRNA (Sussman & Kim, 1976), and also there are several tertiary interactions (A9 forming a triple with UA12, m^7G46 forming a triple with CG13, etc.) which presumably do not occur in the isolated fragment. The resonance position of CG13 in the fragment is shifted upfield by stacking with A14, which may not be the same in the intact tRNA; the calculated position shown by the bar on the *x* axis assumes a full stack with A14. The specific DHU stem resonance positions are further corroborated by the fact that this four base pair helix is preferentially lost upon raising the temperature as shown in the lower spectrum of Figure 9. The intensity losses at −13.9, −13.3, and −11.8 ppm are clearly attributable to base pairs 12, 11, and 13, respectively. A further interesting point in Figure 9 is the presence of an additional resonance at either −12.5 or −12.3 ppm (depending on whether the uncertain resonance from CG27 is assigned at −12.3 or −12.5 ppm). A possible candidate for such a resonance is the Pur26–Pur44 interaction, which is seen crystallographically and involves a ring NH bond between two purines which are not coplanar (Sussman & Kim, 1976). In the intact tRNA, residue 26 and residue 44 are intercalated between GC10 and CG27, forming a continuous helix from the combined anticodon and DHU helixes (Sussman & Kim, 1976); the present data are consistent with this orientation

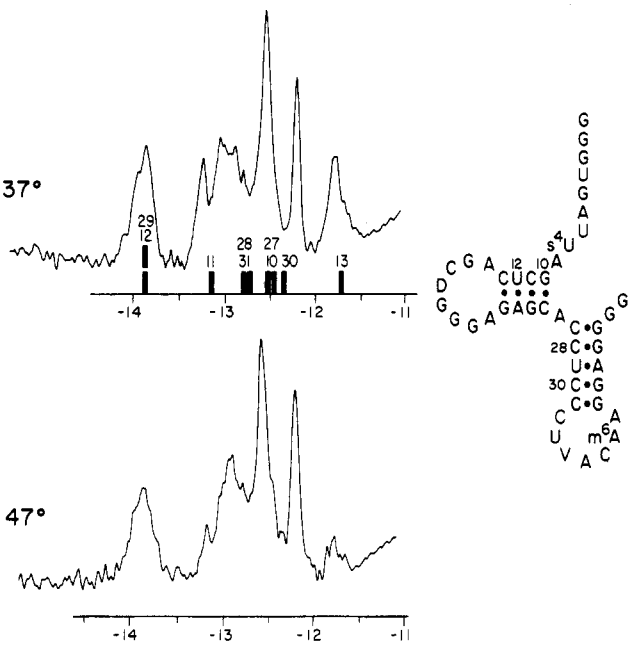

FIGURE 9: NMR spectra of fragment 1–45 of *E. coli* $tRNA_1^{Val}$ containing the DHU helix and the anticodon helix at 37 and 47 °C in 5 mM sodium phosphate and 100 mM NaCl, pH 7.0.

being maintained in fragments containing these two helixes.

Unfortunately, it is not possible to obtain helical hairpin fragments of the acceptor stem. To investigate whether the resonances from this helix can be satisfactorily accounted for on the basis of 11-fold helix ring current shift analysis, we sought a tRNA species with an exceptionally stable amino acid acceptor stem. We reasoned that in such a species it might be possible at some relatively high temperature to melt out all other base pair interactions in the intact tRNA, thus leaving only the acceptor stem resonances at experimentally determinable positions. Our best candidate for such a role is *E. coli* $tRNA^{Phe}$; this species contains six consecutive GC pairs in its acceptor stem with a seventh AU base pair at the base of this helix. The spectra, at three temperatures, of *E. coli* $tRNA^{Phe}$ are shown in Figure 10. At 55 °C the majority of the resonances observed at 35 °C are still present in the spectrum and the initial broadening of the weakest resonances has just begun to occur. At 68 °C there remain six sharp resonances from the acceptor stem plus a seventh severely broadened resonance at −13.8 ppm; this latter resonance from the terminal AU7 regains intensity upon lowering the temperature to 66 °C. The positions of the six sharp resonances are −13.2, −12.75, −12.55, −12.55, −12.4, and −12.3 ppm. The predicted positions for base pairs 2, 3, 1, 4, 5, and 6 are −13.05, −12.77, −12.52, −12.50, −12.46, and −12.31 ppm, respectively. Thus, the agreement is quite good and we feel that acceptor helixes in tRNA can also be successfully predicted to within ~0.1 ppm by using the assumption of 11-fold helix geometry. Thus, in addition to experimentally assigning the majority of the secondary helical resonances in $tRNA_1^{Val}$, we have established that the Arter & Schmidt (1976) ring current shift values for 11-fold helixes are reasonably accurate in predicting tRNA secondary resonances for anticodon helixes, rT helixes, and acceptor helixes when used in conjunction with an AU° value of −14.35 ppm and GC° values of −13.45 to −13.4 ppm. We have also experimentally assigned the secondary resonances in *E. coli* $tRNA^{Lys}$ and *E. coli* $tRNA^{Phe}$ from hairpin helixes dissected from these molecules; in these cases also the agreement between the theoretically predicted tRNA spectrum and the experimentally assigned spectrum is quite good. We

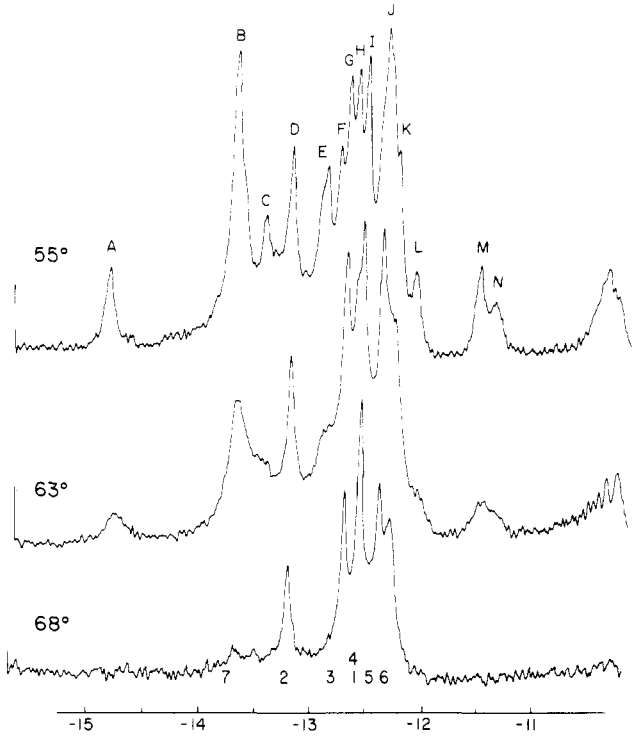

FIGURE 10: Low-field NMR spectra of *E. coli* $tRNA^{Phe}$ in 10 mM sodium cacodylate, 100 mM NaCl, and 15 mM $MgCl_2$, pH 7.0, at elevated temperature. This tRNA contains a very stable acceptor helix of six consecutive GC pairs with a terminal AU pair (see Figure 13); at 68 °C only the six GC resonances remain in the spectrum with a broadened resonance from AU7 which reappears upon lowering the temperature to 66 °C. The numbers represent peak assignments to the acceptor helix base pairs based on neighboring ring current shifts as described in the text.

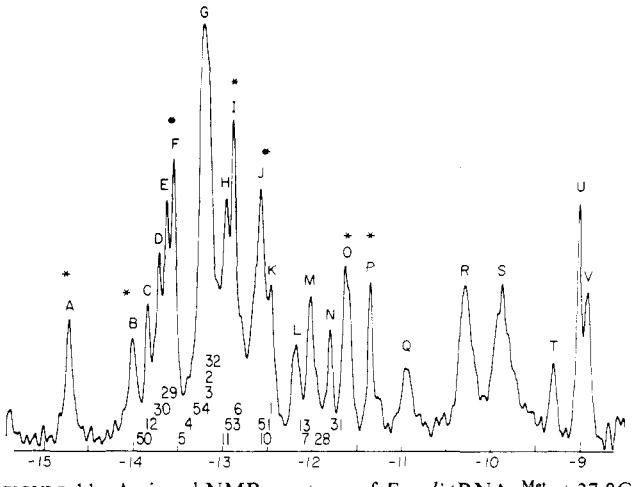

FIGURE 11: Assigned NMR spectrum of *E. coli* $tRNA_m^{Met}$ at 37 °C in 10 mM sodium cacodylate, 100 mM NaCl, and 15 mM $MgCl_2$, pH 7.0. The assignment of secondary Watson–Crick base pairs is based on the calibrated sequence-dependent ring current shift effects described in the text. Additional resonances are designated by asterisks.

next turned to comparative analysis of predicted resonances in other related tRNA species.

As shown in Figure 5, there are seven or eight extra resonances in $tRNA_1^{Val}$ between −11 and −15 ppm which cannot be assigned to secondary Watson–Crick base pairs in the cloverleaf structure. The spectrum of *E. coli* $tRNA_m^{Met}$ is shown in Figure 11. The predicted secondary resonances are indicated on the spectrum by their base pair number; again we observe a set of extra resonances at positions similar to the tertiary resonances in $tRNA_1^{Val}$. Tertiary resonances are also

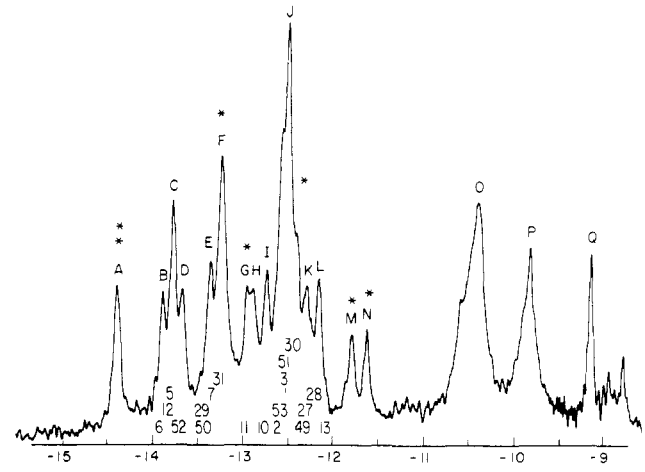

FIGURE 12: Assigned NMR spectrum of yeast $tRNA^{Phe}$. Secondary base pair assignments are based on calibrated ring current shift predictions and our previously published fragment spectra. Extra resonances are designated by asterisks.

observed at these positions in the spectra of *E. coli* $tRNA_{2A}^{Val}$, *E. coli* $tRNA_{2B}^{Val}$, and *E. coli* $tRNA_3^{Gly}$. Since yeast $tRNA^{Phe}$ is the only tRNA for which the tertiary base pairing interactions are known with precision, we also analyzed this spectrum in the same way. The results are shown in Figure 12. Again a similar set of additional resonances is observed, but in this case resonance A is at −14.3 ppm instead of −14.9 ppm; we have previously noted (Reid et al., 1975) that bacterial tRNAs containing s^4U8 contain a resonance at −14.9 ppm which is moved upfield to −14.3 ppm in yeast tRNAs which contain U8.

Discussion

A distinct advantage of the NMR approach to analyzing the solution structure of tRNA is that many related tRNA species can be studied and compared in a reasonable period of time. Unfortunately, there is only one tRNA, namely, yeast phenylalanine tRNA, for which the detailed three-dimensional structure in the crystalline state is known. In this work, and in the following three papers (Hurd & Reid, 1979a,b; Hurd et al., 1979), we have analyzed the solution structure of yeast phenylalanine tRNA in light of the crystal structure of this molecule and made the further assumption that closely related tRNA species, containing the same number of residues in the various loops and helixes, adopt the same tertiary structure. The results presented here corroborate our earlier claims of 7 ± 1 extra resonances over and above the 20 resonances from secondary Watson–Crick base pairs in the low-field NMR spectrum of several tRNAs. A combination of experimental assignment of secondary resonances from helical fragments, ring current prediction of secondary resonance positions, and observation of temperature-sensitive and magnesium-sensitive resonances in the $tRNA_1^{Val}$ spectrum all strongly implicate six specific resonances as being derived from ring NH hydrogen bonds of tertiary interactions. A more interesting observation is that the position of this set of six tertiary resonances is remarkably similar in different tRNAs (e.g., yeast $tRNA^{Phe}$, *E. coli* $tRNA_1^{Val}$, $tRNA_m^{Met}$, and $tRNA_{2A}^{Val}$, etc.). The chemical shift of these tertiary resonances, even in species with limited primary sequence homology, is −14.8 ± 0.1 (−14.3 in species with U8 instead of s^4U8), −14.1 ± 0.2, −13.4, −12.9, ca. −12.2, and ca. 11.5 ppm. The relatively constant position of the tertiary base pair resonances might at first appear surprising, but we had hoped for such a result from our design of these experiments. The majority of tertiary

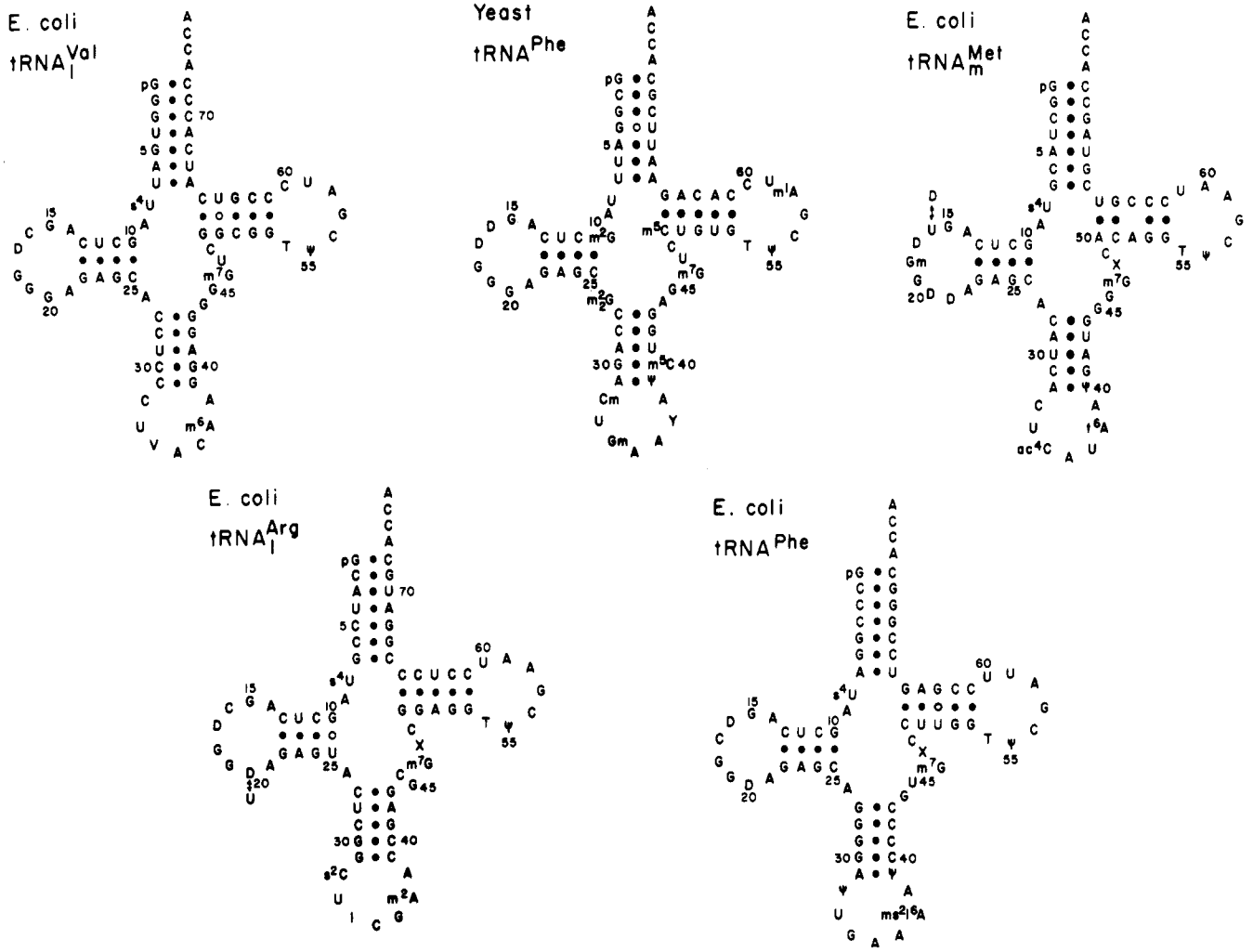

FIGURE 13: Sequences of the tRNA species, arranged in the classical cloverleaf structure, used in this study.

interactions in the crystal structure of yeast tRNA^{Phe} involve hydrogen bonding to the DHU helix and stacking of additional base pairs at the ends of this helix. For instance A14–U8 is stacked on the terminal CG13 of the DHU helix and G15–C48 is stacked on the 14–8 base pair (Sussman & Kim, 1976). Furthermore, m^{7}G46 is bonded to CG13 of the DHU helix, C56 is bonded to G19 of the DHU loop, and Pur26–Pur44 is stacked on GC10 at the internal terminus of the DHU helix. Since the DHU helix largely defines the environment of these tertiary hydrogen bonds, we chose a series of tRNAs with an identical sequence of base pairs in this helix (see Figure 13) in the hope of maintaining a similar ring current shift environment for the extra tertiary interactions. We reemphasize that the rationale of this approach depends on the assumption that these other tRNAs fold in the same manner as yeast tRNA^{Phe}; in support of this assumption persuasive arguments for the generality of tRNA folding based on coordinated base changes in a variety of tRNA sequences have already been presented by others (Kim et al., 1974a,b; Klug et al., 1974). The consistency of our comparative data indicating similarity of the tertiary resonance positions can be interpreted conversely as experimental support for these hypotheses.

A further important result from the experiments presented here is the calibration of a newly published method of calculating ring current shift values for RNA helixes. When the published ring current values for an 11-fold helix pitch (Arter & Schmidt, 1976) are used in conjunction with our experimentally calibrated AU° and GC° starting chemical shifts, the agreement between predicted low-field spectra and experimentally observed spectra of short RNA hairpin helixes is remarkably good. The spectrum of the intact tRNA$_1^{Val}$ cloverleaf resonances predicted by this method agrees quite well with the secondary cloverleaf resonances experimentally assigned from the individual component helixes dissected out of this tRNA and analyzed separately. In data not shown here, the agreement between the *E. coli* tRNA^{Phe} and *E. coli* tRNA^{Lys} spectra assigned experimentally from their component fragment spectra and the assignments of the intact tRNA spectrum based on 11-fold ring current shift predictions is also quite good. The actual geometry of the major helixes in the crystal structure of tRNA is close to, but not exactly the same as, a regular 11-fold RNA screw pitch (Sussman & Kim, 1976; Jack et al., 1976), and this structural irregularity may explain part of the discrepancy since the predictive rules are based on regular 11-fold geometry. Our experimental results have convinced us that the method of predicting and assigning secondary resonances shown in Table I and Figure 5, although not perfect, is nevertheless a very useful method for interpreting low-field NMR spectra of RNA. The method of Robillard et al. (1976), in which the net ring current shift of all nucleotides in tRNA on a given ring NH proton is calculated from the atomic coordinates of the tRNA crystal structure, is undoubtedly more refined than our own approach. However, the fact that all residues more distant than the next-to-nearest neighbors contribute less than 10% of the net ring current shift on a given proton suggests that the two

methods should agree to 90% or better. Although Robillard et al. (1976) used ring currents calculated by Haigh & Mallion (1971) whereas the Arter & Schmidt (1976) values we have used are derived from ring currents calculated by Giessner-Prettre & Pullman (1970), the value for the net upfield ring current shift of a ring NH proton in any given environment of nearest and next-to-nearest neighbors is very similar in both methods (G. T. Robillard, personal communication). Furthermore, in order to fit our experimental spectrum of yeast $tRNA^{Phe}$, Robillard et al. (1976) were forced to use starting AU° and GC° resonance positions which were within 0.1 ppm of the −14.35- and −13.45-ppm values which we have experimentally established.

In the three-dimensional structure of yeast $tRNA^{Phe}$ (and presumably $tRNA_1^{Val}$, $tRNA_{2A}^{Val}$, $tRNA_m^{Met}$, etc.) the tertiary interactions which unambiguously involve ring NH hydrogen bonds are U8–A14, G19–C56, m^7G46–G22, T54–A58, and G15–C48 (Sussman & Kim, 1976; Robertus et al., 1974; Quigley & Rich, 1976). We submit that these interactions are maintained in solution and are responsible for 5 of the 7 ± 1 additional resonances which we have detected at constant positions in the low-field NMR spectra of several class 1 D4V5 tRNA species. More ambiguous, in terms of generating a resonance in the −11- to −15-ppm NMR spectrum, are the non-coplanar m_2^2G26–A44 (which may not generate a ring NH bond in species with A26 and G44) and G18–Ψ55, which may not involve the G18 N1H proton. A further complication is the crystallographically observed ring NH hydrogen bond from Ψ55 to phosphate; we have no precedent for estimating the chemical shift of a hydrogen bond to phosphate but would guess that it would resonate toward the high-field end of the spectrum. In this connection it is interesting that peaks U, V, and W between −9.4 and −10.6 ppm in Figure 1 are also broadened and decreased during the early thermal transitions, which we attribute to tertiary unfolding; these three resonances are most likely ring NH protons involved in tertiary hydrogen bonding, and their lack of downfield shift may well be due to atypical hydrogen-bond acceptors such as phosphates or ribose OH groups.

A final point worth reemphasizing is that all of our "additional" resonances are not necessarily derived from tertiary interactions. Most of the tRNAs we have studied contain one GU pair in their cloverleaf structure which is not included in the predicted resonances from secondary Watson–Crick pairs. The GU-containing rT helix of $tRNA_1^{Val}$ suggests that, in this tRNA, the GU pair contributes at least one, and probably two, protons between −11 and −12 ppm. More recent studies, to be published elsewhere, utilizing the nuclear Overhauser effect reveal that peaks Q and T (−11.9 and −11.35 ppm in Figures 1, 2e, and 5) are the two hydrogen-bonded protons of GU50 (P. D. Johnston and A. G. Redfield, personal communication; R. E. Hurd and B. R. Reid, unpublished experiments). From the chemical shifts shown in Figure 4, we tentatively assign U64 N3H to peak Q and G50 N1H to peak T. Since these two peaks are derived from the secondary cloverleaf, this now leaves only five or six bona fide tertiary resonances in the −11- to −15-ppm region.

In the following series of papers (Hurd & Reid, 1979a,b; Hurd et al., 1979) we shall assign four of the tertiary interactions to their specific low-field NMR resonance by a combination of chemical, biochemical, and comparative spectroscopic methods.

Acknowledgments

We thank the advisory committee for awarding time on the Bruker HXS-360 instrument to this project, and special thanks are due to Dr. W. W. Conover at SMRL for his advice and helpfulness.

References

Arter, D. B., & Schmidt, P. G. (1976) *Nucleic Acids Res. 3*, 1437.

Bolton, P. H., & Kearns, D. R. (1976) *Nature (London) 262*, 423.

Bolton, P. H., Jones, C. R., Bastedo-Lerner, D., Wong, K. L., & Kearns, D. R. (1976) *Biochemistry 15*, 4370.

Dadok, J., & Sprecher, R. F. (1974) *J. Magn. Reson. 13*, 243.

Daniel, W. E., & Cohn, M. (1975) *Proc. Natl. Acad. Sci. U.S.A. 72*, 2582.

Englander, S. W., & Englander, J. J. (1965) *Proc. Natl. Acad. Sci. U.S.A. 53*, 370.

Geissner-Prettre, C., & Pullman, B. (1970) *J. Theor. Biol. 27*, 87.

Gillam, I., Millward, S., Blew, D., Von Tigerstrom, M., Wimmer, E., & Tener, G. M. (1967) *Biochemistry 6*, 3043.

Haigh, C. W., & Mallion, R. B. (1971) *Mol. Phys. 22*, 955.

Holmes, W. M., Hurd, R. E., Reid, B. R., Rimerman, R. A., & Hatfield, G. W. (1975) *Proc. Natl. Acad. Sci. U.S.A. 72*, 1068.

Hurd, R. E., & Reid, B. R. (1979a) *Biochemistry* (following paper in this issue).

Hurd, R. E., & Reid, B. R. (1979b) *Biochemistry* (fourth of four papers in this issue).

Hurd, R. E., Azhderian, E., & Reid, B. R. (1979) *Biochemistry* (third of four papers in this issue).

Jack, A., Ladner, J. E., & Klug, A. (1976) *J. Mol. Biol. 108*, 619.

Jones, C. R., & Kearns, D. R. (1974) *Proc. Natl. Acad. Sci. U.S.A. 71*, 4237.

Jones, C. R., & Kearns, D. R. (1975) *Biochemistry 14*, 2660.

Jones, C. R., Kearns, D. R., & Muench, K. (1976) *J. Mol. Biol. 103*, 747.

Katz, L., & Penman, S. (1966) *J. Mol. Biol. 15*, 220.

Kearns, D. R. (1976) *Prog. Nucleic Acid Res. Mol. Biol. 18*, 91.

Kearns, D. R., & Shulman, R. G. (1974) *Acc. Chem. Res. 7*, 33.

Kearns, D. R., & Wong, Y. P. (1975) *J. Mol. Biol. 87*, 755.

Kearns, D. R., Patel, D., & Shulman, R. G. (1971a) *Nature (London) 229*, 338.

Kearns, D. R., Patel, D., Shulman, R. G., & Yamane, T. (1971b) *J. Mol. Biol. 61*, 265.

Kim, S. H., Suddath, F. L., Quigley, G. J., McPherson, A., Sussman, J. L., Wang, A. H. J., Seeman, N. C., & Rich, A. (1974a) *Science 185*, 435.

Kim, S. H., Sussman, J. L., Suddath, F. L., Quigley, G. J., McPherson, A., Wang, A. J. H., Seeman, N. C., & Rich, A. (1974b) *Proc. Natl. Acad. Sci. U.S.A. 71*, 4970.

Klug, A., Ladner, J., & Robertus, J. D. (1974) *J. Mol. Biol. 89*, 511.

Nishimura, S. (1971) in *Procedures in Nucleic Acid Research* (Cantoni, G. L., & Davies, D. R., Eds.) Vol. 2, p 542, Harper and Row, New York.

Quigley, G. J., & Rich, A. (1976) *Science 194*, 796.

Reid, B. R. (1976) *Nature (London) 262*, 424.

Reid, B. R., & Robillard, G. T. (1975) *Nature (London) 257*, 287.

Reid, B. R., Einarson, B., & Schmidt, J. (1972) *Biochimie 54*, 325.

Reid, B. R., Ribeiro, N. S., Gould, G., Robillard, G., Hilbers, C. W., & Shulman, R. G. (1975) *Proc. Natl. Acad. Sci. U.S.A. 72*, 2049.
Reid, B. R., Ribeiro, N. S., McCollum, L., Abbate, J., & Hurd, R. E. (1977) *Biochemistry 16*, 2086.
Robertus, J. D., Ladner, J. E., Finch, J. T., Rhodes, D., Brown, R. S., Clark, B. F. C., & Klug, A. (1974) *Nature (London) 250*, 546.
Robillard, G. T., Tarr, C. E., Vosman, F., & Berendsen, H. J. C. (1976) *Nature (London) 262*, 363.
Simsek, M., Petrissant, G., & RajBhandary, U. L. (1973) *Proc. Natl. Acad. Sci. U.S.A. 70*, 2600.
Shulman, R. G., Hilbers, C. W., Kearns, D. R., Reid, B. R., & Wong, Y. P. (1973) *J. Mol. Biol. 78*, 57.
Stout, C. D., Mizuno, H., Rao, S. T., Swaminathan, P., Rubin, J., Brennan, T., & Sundaralingam, M. (1978) *Acta Crystallogr., Sect. B 34*, 1529.
Sussman, J. L., & Kim, S. H. (1976) *Science 192*, 853.
Wong, K. L., Kearns, D. R., Wintermeyer, W., & Zachau, H. G. (1975a) *Biochim. Biophys. Acta 395*, 1.
Wong, K. L., Wong, Y. P., & Kearns, D. R. (1975b) *Biopolymers 14*, 749.
Wong, K. L., Bolton, P. H., & Kearns, D. R. (1975c) *Biochim. Biophys. Acta 383*, 446.

Nuclear Magnetic Resonance Studies on Transfer Ribonucleic Acid: Assignment of AU Tertiary Resonances†

Ralph E. Hurd and Brian R. Reid*

ABSTRACT: The hydrogen-bonded ring NH nuclear magnetic resonance (NMR) spectra of several transfer ribonucleic acid (tRNA) species have been examined with particular emphasis on the extreme low-field portion. Between −13.8 and −15 ppm there are two extra resonances which are not derived from cloverleaf base pairs. A combined approach involving undermodified tRNAs, chemical modification, and hairpin fragment studies has assigned the T54–A58 resonance at −14.3 ppm in yeast $tRNA^{Phe}$ and *Escherichia coli* $tRNA_1^{Val}$; the U8–A14 resonance has been assigned at −14.3 ppm, and the s^4U8–A14 resonance in bacterial tRNAs has been assigned at −14.9 ppm. The T54–A58 resonance shifts between −14.3 and −13.8 ppm depending on the surrounding nucleotide sequence in the ribothymidine loop.

In an earlier paper we showed that several different class 1 D4V5 tRNA[1] species contain six to seven extra resonances derived from tertiary base pairing in their low-field (−11 to −15 ppm) NMR spectra (Reid et al., 1977). In an accompanying paper in this series we have used several independent methods to identify which resonances in the 26- to 27-proton spectra were derived from tertiary base pairs [see Reid et al. (1979)]. An interesting result from these studies was that several tRNAs with the same tertiary folding potential (Kim et al., 1974; Klug et al., 1974) as yeast $tRNA^{Phe}$ exhibited tertiary NMR resonances with chemical shifts similar to those observed for the yeast $tRNA^{Phe}$ tertiary resonances. Candidates for these extra low-field NMR resonances are the hydrogen-bonded ring NH protons of the following tertiary base pairs observed in the three-dimensional folding of yeast $tRNA^{Phe}$: 8–14, 54–58, 46–22, 19–56, 15–48, and possibly 26–44 and/or 18–55 (Sussman & Kim, 1976; Quigley & Rich, 1976; Jack et al., 1976). Two of these interactions involve AU-type base pairing, namely, U8 (s^4U8)–A14 and rT54–A58; the remaining tertiary interactions involving ring NH protons are GC-type interactions in that they involve hydrogen bonding of the G N1H proton. We have previously shown that AU base pairs resonate to lower field than GC base pairs because of the greater inherent deshielding of U N3H compared to G N1H [see Reid et al. (1979)]. This observation suggested that the U8 (s^4U8)–A14 interaction and the rT54–A58 interaction should each generate a resonance in the extreme low-field region of the low-field spectrum.

In this paper we have used a combination of helical RNA fragment analysis, chemical modification, and comparative spectroscopy to assign the resonances from U8 (s^4U8)–A14 and rT54–A58. In subsequent papers (Hurd & Reid, 1979; Hurd et al., 1979) we will assign the guanosine-type tertiary interaction in the low-field NMR spectrum.

Materials and Methods

Isolation of tRNA. *E. coli* $tRNA_1^{Val}$ (Reid et al., 1979) and *E. coli* $tRNA^{fMet}$ (Reid et al., 1977) were purified to homogeneity as described previously. The final preparations accepted over 1800 pmol of valine and methionine/A_{260} unit, respectively, when aminoacylated with the corresponding pure aminoacyl-tRNA synthetase enzymes. *E. coli* $tRNA_1^{Gly}$ and $tRNA_3^{Gly}$ were initially separated by BD-cellulose chromatography according to the procedure of Gillam et al. (1967). *E. coli* $tRNA_1^{Gly}$ eluted extremely early in the gradient followed closely by $tRNA_2^{Gly}$; the major glycine species, $tRNA_3^{Gly}$, eluted much later in the gradient at ~0.82 M NaCl. The $tRNA_1^{Gly}$ fraction was purified to homogeneity by DEAE-Sephadex chromatography (Nishimura, 1971); the $tRNA_3^{Gly}$ fraction was purified to homogeneity by DEAE-Sephadex chromatography, Sepharose 4B chromatography (Holmes et al., 1975), and RPC5 chromatography (Pearson

† From the Biochemistry Department, University of California, Riverside, California 92521. *Received August 10, 1978; revised manuscript received May 29, 1979.* Supported by grants from the National Science Foundation (PCM73-01675), the American Cancer Society (NP-191), and the National Cancer Institute, Department of Health, Education and Welfare (CA11697). The 360-MHz NMR spectra were obtained on a modified Bruker HXS-360 spectrometer at the Stanford Magnetic Resonance Laboratory supported by National Science Foundation Grant No. GR23633 and National Institutes of Health Grant No. RR00711.

[1] Abbreviations used: tRNA, transfer ribonucleic acid; DHU, dihydrouridine; rT, ribothymidine; m^7G, N^7-methylguanosine; Ψ, pseudouridine; s^4U, 4-thiouridine; EDTA, ethylenediaminetetracetic acid; NMR, nuclear magnetic resonance; BD-cellulose, benzoylated DEAE-cellulose.

0006-2960/79/0418-4005$01.00/0